Article:
Gevaudan, JP, Santa-Ana, B and Srubar III, WV (2021) Iron mineral admixtures improve the sulfuric acid resistance of low-calcium alkali-activated cements. Cement and Concrete Composites, 116. 103867. ISSN 0958-9465

https://doi.org/10.1016/j.cemconcomp.2020.103867

Iron Mineral Admixtures Improve the Sulfuric Acid Resistance of Low-Calcium Alkali-Activated Cements

Juan Pablo Gevaudan [1], *Briana Santa-Ana*[1], *Wil V. Srubar III* [1,2,†]

[1]Department of Civil, Environmental, and Architectural Engineering, University of Colorado Boulder, 1111 Engineering Drive, ECOT 441 UCB 428, Boulder, Colorado USA 80309. [2]Materials Science and Engineering Program, University of Colorado Boulder, 4001 Discovery Drive, Room N378, Boulder, Colorado USA 80303. [†]Corresponding Author: wsrubar@colorado.edu

Abstract

We investigated the sulfuric acid resistance of low-calcium alkali-activated materials (*i.e.*, geopolymers) supplemented with an iron mineral admixture (*i.e.*, hematite). Geopolymers without and with 5% hematite were produced at two alkali contents (Na:Al = 0.86 and 1.39). Acid degradation reactions were comprehensibly studied through three replenishes of acid. Results demonstrate that hematite is chemically active upon acid exposure yielding a short-term increase in acid neutralization capacity. Prolonged acid resistance was enhanced in high alkali content formulations with hematite. Acid exposure revealed minimal changes to mineralogy, molecular structure, and micro-scale porosity in these samples, resulting in less dealumination and silicon leaching. Thus, results indicate that the acid buffering capacity of geopolymers, specifically at higher alkali content formulations, increases due to the addition of hematite. The increased buffering capacity leads to lower degrees of dealumination of the N-A-S-H cementitious binder. These results are important to explain the increased acid durability of alkali-activated materials synthesized from industrial aluminosilicate precursors (*e.g.,* slag, fly ash, lateritic clays) that may contain iron minerals.

Keywords: Sulfuric Acid, Alkali-Activated Cements, Geopolymers, Microbial-Induced Concrete Corrosion

1.0 Introduction

A global need to improve the resilience and sustainability of civil infrastructure has prompted a recent interest in developing durable, low-CO_2 concrete technology. Microbial-induced concrete corrosion (MICC) in subterranean infrastructure is a major durability challenge. In the United States alone, local governments spend approximately $50 billion annually to mitigate the effects of microbially-produced sulfuric acid in more than 800,000 miles of sewers [1], [2]. MICC consists of three main stages, namely: (1) carbonation of the surface ($9 < pH < 10$); (2) establishment of a microbial biofilm ($4 < pH < 5$); and, (3) severe corrosion due to sulfuric acid ($pH < 2$) [3]. Hence, concrete materials that can withstand such aggressive acidic environments are of interest. Toward this aim, alkali-activated cements (AACs) have been proposed as a possible material solution to this pervasive durability challenge. AACs are a class of low-CO_2, acid-resistant alternatives to portland cement-based materials. The lower environmental impact of AACs compared to portland cement-based materials has been previously reported in [4]–[6]. Similarly, the superior acid resistance of AACs has been discussed extensively in previous research [7]–[9]

The acid resistance of AACs is primarily dependent on both the chemical composition of the microstructure (i.e., Ca:Si, Al:Si) and the permeability of the porous network [10], [11]. A recent comparison between two different AACs, slag activated vs. fly ash activated materials, revealed that slag-activated mortars, which contain higher calcium contents, could better withstand the MICC aggressive environment due to their low gas permeability when compared to fly ash activated materials. More specifically, activated slag mortars with a lower permeability were found to have lower rates of carbonation and H_2S acidification in aggressive sewer conditions during the initial stages of MICC [12]. The lower

permeability in AACs has also been shown to contribute to lower microbial respiration rates, which limit the establishment of microbial biofilms in the second stage of MICC [13]. However, much research considers the third stage of MICC and is simulated as sulfuric acid exposures [14]. Results from these sulfuric solution experiments have revealed decreases in overall degradation correlated with lower calcium content [15], suggesting that low-calcium AACs from metakaolin or low-calcium fly ashes are more acid resistant than calcium-rich AACs produced from ground-granulated blast furnace slags (GBFS). However, as noted earlier, these rates of degradation, especially in calcium-rich AACs, can be attenuated by a slow diffusion process that is facilitated by complex porous networks. Pore-filling and macropore structures (>100 nm) help reduce mesoporous structure (2-50 nm) and, as a result, decreases the rate of degradation [16].

The authors have recently proposed a new theory of acid degradation in AACs. Acid degradation of low-calcium AACs (*i.e.*, geopolymers) involves an ion-exchange reaction between the charge-stabilizing cations (*e.g.*, sodium, Na^{+}) of the aluminosilicate cementitious binder (Si-O-Al) and hydronium (H_3O^{+}). Association of the hydronium with the localized negative charge in aluminosilicate cementitious binders results in an electrophilic attack, which ejects tetrahedral aluminum (Al) in a process named dealumination [10]. Dealumination is concurrent with incorporation of silicon (Si) species, which, depending on chemical composition of the pore solution (e.g., internal pH), precursor chemistry (i.e., CaO content) and degree of Al-crosslinking (e.g., SiO_2:Al_2O_3 ratio) can enable the formation of a silica gel network, as reported by [17]. The formed gel network is suggested to play an important role in the durability of these materials, as it may inhibit further diffusion of aggressive agents [18].

Recently, the authors showed experimentally that Cu^{+2} and Co^{+2}, as well as other cations, incorporated in AACs exhibited mobility during acid exposure, accumulated at the reaction front, and aided in increasing the acid resistance through a process termed *polyvalent cationic stabilization* of the aluminosilicate binder [19]. However, initial experimental results were observed in slag-based AACs that contained a variety of mineral phases that became chemically active during acid exposure. Such complexity can confound mechanistic understanding due to simultaneous inter-ionic interactions. Hence, direct evidence on the role of Cu^{+2}, Co^{+2}, and other metallic cations, like iron (Fe), in pure aluminosilicate systems is essential to isolate specific ionic interactions to elucidate mechanistic understanding of their fundamental behavior related to acid degradation.

Previous work on acid-attacked fly-ash AACs with high Fe contents (>48%) demonstrated high mass loss when compared to portland cement paste [20]. The content of Fe (as Fe_2O_3) in slag and fly ash has been reported to be 0.4-1.8 wt.% and 3.2-18.1 wt.%, respectively [21]–[24]. Traditional mass loss measurements, however, have been shown by [25] to not necessarily correlate with chemical acid degradation. In addition to the limits in measurements, the presence of mineral phases in AACs obfuscates the explicit role of chemically active phases during acid attack. For example, recent research by [26] found that alkali-activated impure metakaolin containing iron minerals demonstrated improved acid resistance to similar formulations utilizing pure metakaolin. Similar results have been reported for slag-based AACs with Fe-rich additions [27]. Hence, these recent results elucidate critical gap in knowledge in the understanding of the explicit role that mineral impurities have on the acid attack of AACs. To this aim this study investigates the role of Fe in the acid degradation of low-calcium metakaolin-based AACs.

2. Materials and Experimental Methods

2.1 Materials

High purity metakaolin (MK) (MetaMax) was supplied by BASF Chemical Corporation (Georgia, USA). The MK had a Si:Al ratio of unity (1.0), determined *via* ICP-OES, and an average particle size of 1.3µm. Hematite (Fe_2O_3) average particle diameter of 0.18 µm was supplied by Strem Chemicals Inc. with a chemical purity of 99.8%. Alkali-activating solutions were prepared using sodium hydroxide (Sigma-Aldrich, NaOH ≥ 97%) and sodium silicate (NaSi, Sigma-Aldrich, SiO_2 = 27 wt. %, Na_2O = 11 wt. %). More specifically, high-density polyethylene (HDPE) 500ml bottles were used to mix NaSi, NaOH, and

H_2O proportions in **Table 1.** Sulfuric acid solution with a pH of 2.0 ± 0.07 was prepared by adding sulfuric acid (Sigma-Aldrich, $H_2SO_4 \geq 95\%$) to deionized water.

2.2 Experimental Methods

2.2.1 AAC Sample Preparation

Geopolymer samples were produced with two alkaline activators to achieve Na:Al atomic ratios of 0.86 and 1.39 with a uniform Si:Al atomic ratio of 1.15 (see **Table 1**). Alkali-activating solutions were prepared in high-density polyethylene bottles, which were sealed and cooled for one hour at 4 °C to enable the NaOH exothermic reaction to subside. The effect of iron mineral admixtures was explored with the addition of 5 wt.% of hematite [28]. MK was alkali-activated with the respective alkaline solutions and mixed for three minutes with one minute of manual mixing, one minute of mechanical mixing, followed by one final minute of manual mixing. Mixtures achieved a homogenous consistency after the mixture procedure and were placed in Vaseline-lubricated molds (diameter: 13mm, height: 25mm). Subsequently, mixtures were tamped for 30 seconds and vibrated for 30 seconds until visible entrapped air was removed. Paste samples were then cured in sealed containers (99% RH) in a Quincy forced air laboratory oven for 48 hours at 40°C. After initial curing, samples were dried at 40°C for an additional 24 hours.

Table 1. Mixture proportions for MK-based AAC control and iron supplemented samples.

	Constituent Materials					Important Parameters		
Sample Name	**MK (g)**	**Fe_2O_3 (g)**	**NaSi (g)**	**NaOH (g)**	**H_20 (g)**	**Fe (%)**	**Si:Al**	**Na:Al**
Control Low	50	0	13	9.4	33	0	1.15	0.86
Control Low + Fe	50	2.6	13	9.4	33	5	1.15	0.86
Control High	50	0	13	15.8	33	0	1.15	1.39
Control High + Fe	50	2.6	13	15.8	33	5	1.15	1.39

2.2.2 Acid Exposure and Leaching

Samples (diameter: 13mm, height: 20mm) were exposed three times to a sulfuric acid solution with a pH of 2.0 ± 0.07 until pH equilibrium was attained (< 0.0025 pH/hour). Following a modified ASTM C1308 methodology, samples were suspended using a 46 mm Savillex support screen (730-0046) and constantly stirred in the acid solution. The volume-to-surface-area ratio of the solution and AAC sample was held constant at 10. A magnetic stirrer was used to ensure homogenous solution mixing. pH equilibrium was defined as the time in which the recorded change in pH was < 0.0025 per hour. pH values were obtained using a Mettler Toledo benchtop F20 pH/mV meter. The pH probe was calibrated using a three-point curve with proper bracketing with reference solutions of pH values 2.0, 7.0, 10.1, and 12.01. After equilibrium was reached, the acid solutions were replaced, and samples of the leachate media were analyzed *via* ICP-MS. Leachate media contained silica suspensions. To ensure proper analysis, samples were first acid digested to dissolve any colloidal or aggregated particles or gels and subsequently run against blank. Three separate standards were made to test the accuracy of the results by diluting certified standards. Triplicates of each sample were exposed to acid and aliquots were taken at each equilibrium point.

2.2.3 Fourier-Transform Infrared Spectroscopy (FTIR)

Unexposed and exposed samples were ground in a slurry of ethanol using a McCrone micronizing mill with yttrium-stabilized zirconium (American Elements) grinding beads for five minutes to achieve particle sizes < 5μm. Collected slurries were dried overnight at 60°C. Next, 0.02 ±0.005 grams of each sample were mixed with 2.00 ± 0.050 grams of potassium bromide (KBr) powder and dried at 70 °C. Then, the powder mixtures were homogenized in a Spex Grinder mill and pressed into KBr disk pellets for analysis in a Thermo Scientific Nicolet iS10 FTIR Spectrometer. As a result, KBr disks with sample concentrations of

1% (by weight) were produced. Disks were analyzed against a blank background to remove the absorption spectra from the chamber purged with nitrogen.

2.2.4 Energy Dispersive Spectroscopy (EDS)

The silicon (Si:Fe) and iron (Fe:Al) content of each unexposed and exposed sample were quantified by analyzing the Si Kα, Al Kα, and Fe Kα, which were obtained using a JEOL-8230 electron microprobe with a Thermoscientific energy dispersive spectrometer (EDS). An acceleration voltage of 15 keV and beam current of 20 nA was used for all acquisitions. EDS acquisition was standardless using a spectral acquisition of 15 seconds, which was sufficient to accumulate counts over 4000. A ZAF correction for the elemental matrix was performed in all acquisitions. Twenty randomized points were collected for five different locations in all samples (top, bottom, center, left, and right), totaling an acquisition of 100 EDS points per sample. These points were collected at random to provide an unbiased selection of points and elucidate any general trends of the elemental chemistry and mobility before and after acid exposure. Atomic percentages were quantified and used to discern the central tendencies of bulk Si:Fe and Fe:Al ratios.

2.2.5 X-Ray Diffraction (XRD)

Mineralogy was determined *via* semi-quantitative X-ray diffraction (XRD) using Cu Kα radiation (Siemens D500 X-ray diffractometer). In this methodology, corundum (American Elements) was used as an internal standard to normalize peak heights between samples and align diffraction patterns. AAC samples were powderized and homogenized using a micronizing mill with well-packed yttrium-stabilized zirconium grinding beads. After samples were ground, samples were homogenized in plastic scintillation vials with three Delrin balls. 500 μL of Vertrel cleaning agent (Miller-Stephenson) were added to vials in order to generate aggregates with random particle orientation. Subsequently, samples were sieved through a 250 μm mesh and packed into XRD analysis plates. Samples were then analyzed from 5 to 65 degrees 2θ using Cu Kα X-ray radiation with a step size of 0.02 degrees and a dwell time of 2 seconds per step. Mineralogy was identified using Jade software (MDI, Version 9) and the International Centre for Diffraction Data (ICDD) 2003 database.

2.2.6 Micro-Computerized Tomography (μ-CT)

AAC samples before and after acid exposure were analyzed in a Zeiss Xradia 520 X-ray microscope. Acid-exposed samples were dried in a laboratory oven for at least 12 hours at 40 °C prior to imaging. A micro-computerized tomograph was produced using the 0.4x objective with X-ray source parameters of 60 kV acceleration voltage and 5 Watts. A LE2 filter was utilized to reduce the transmission values between 26% and 40% and maintain intensity counts above 5000. A pixel size resolution of 6.143 ± 0.38 μm was achieved utilizing a pixel averaging of bin one during the acquisition. The tomography images (size: 1.2 cm x 1.1 cm) were reconstructed using a Zeiss reconstruction software to adjust for center-shift and beam hardening artifacts. In addition, ring artifacts from the images were removed using a high-contrast removal operation as well as a despeckling operation to remove pixel defects in the images. Prior to pore-structure segmentation, performed using Dragonfly 3.5, the 32-bit tomography images were pre-processed to correct for noise and uneven grey values within the image. First, a local entropy minimization (node: 9, count: 2) was performed to correct for non-uniform illumination and counteract noise by reducing randomness. Second, an open mathematical morphology operation was performed with a cross structuring element (kernel size: 9) to smooth images and remove isolated pixels. Finally, a median-based smoothing operation was performed to equalize the grey-levels of the image and remove salt-and-pepper noise. Prior to quantification, features of < 1 μm were removed, as these could not be resolved given the pixel-size resolution.

2.2.7 Compressive Strength

An Instron 5869 universal and an MTS Exceed E43-504 (Tension/Compression) testing machine with a 10,000 lbs load cell was employed to test the compressive strength of AAC samples (diameter: 13 mm, height: 20 mm). In order to ensure proper flat testing surfaces, both top and bottom surfaces of AAC samples were smoothed employing 1200 and 2000 abrasive grit sheets. Acid-exposed samples were also tested after two acid exposure cycles. KimWipes™ were used to ensure a saturated surface-dry testing condition. Surface smoothing of these samples was not employed to ensure minimal sample damage. As a result, the compressive strength reported here is likely conservative measurements of the mechanical properties. Moreover, the significance of the compressive strength here is to provide a relative indication of the sample damage due to acid attack in comparison to an unexposed sample of the same dimension and composition. All samples were dimensioned before testing in the load cells and compressed *via* displacement-controlled loading. Between six and eight samples were tested for all samples with the exception of Control High prior to acid exposure which had four samples tested. A higher number of specimens, in comparison to generally accepted triplicates, were tested to provide robust statistical analysis.

3. Results and Discussion

3.1 Mineralogy and Molecular Structure Prior to Sulfuric Acid Exposure

Regardless of Fe content, Control High samples form faujasite (**Figure 1(i)),** while Control Low samples do not exhibit mineral formation, as expected [29]. The presence of faujasite in geopolymer materials, which is well documented [29]–[33], is known to depend on silica availability, alkali content, processing, and curing conditions (*i.e.*, temperature, humidity). The elevated temperature and humidity during curing, along with high concentration of Na^+ cations in the Control High samples, thermodynamically favor formation of faujasite minerals. The authors have previously shown that the mineralization process depends mainly on hydrothermal curing conditions, time, and Na^+ content, which impacts silica availability during geopolymerization. The mineralization of silica-rich zeolites, such as faujasite, in the aluminosilicate binders is important for acid resistance, as it can lower porosity and increase strength in comparison to unmineralized formulations of equal stoichiometry [29], [30].

Control High samples without and with Fe have a higher degree of N-A-S-H crosslinking compared to lower Na:Al counterparts as a consequence of higher alkalinity. Also observed by others, higher precursor dissolution is to be expected, due to a higher concentration of Na^+ cations [34]. Consequently, in Control High samples, there is an increase in Al content and formation of a highly crosslinked geopolymer binder (*i.e.*, N-A-S-H) [34]–[36]. This is evidenced in **Figure 1(ii)** by shifts to lower wavenumbers of both the main Si-O-Al band (1002–1005 cm^{-1}) and the Si-O-Al symmetric-stretching band (720 cm^{-1}) to 984 cm^{-1} and 670 cm^{-1}, respectively [37]. This observation is further supported by strong peaks for in-plane stretching and bending of Si-O and Al-O (460 cm^{-1}), symmetric vibrations of Si-O-Al and Si-O-Si bonds (750 cm^{-1}), and stretching vibrations of Al-O and Si-O tetrahedral (900 cm^{-1}). Control Low samples yield lower absorption intensities for these peaks, signifying lower degrees of reactivity and N-A-S-H crosslinking. Lastly, the presence of carbonates is confirmed for all samples by peaks at1384 cm^{-1} and 1560 cm^{-1}, which correspond to O-C-O asymmetric stretching.

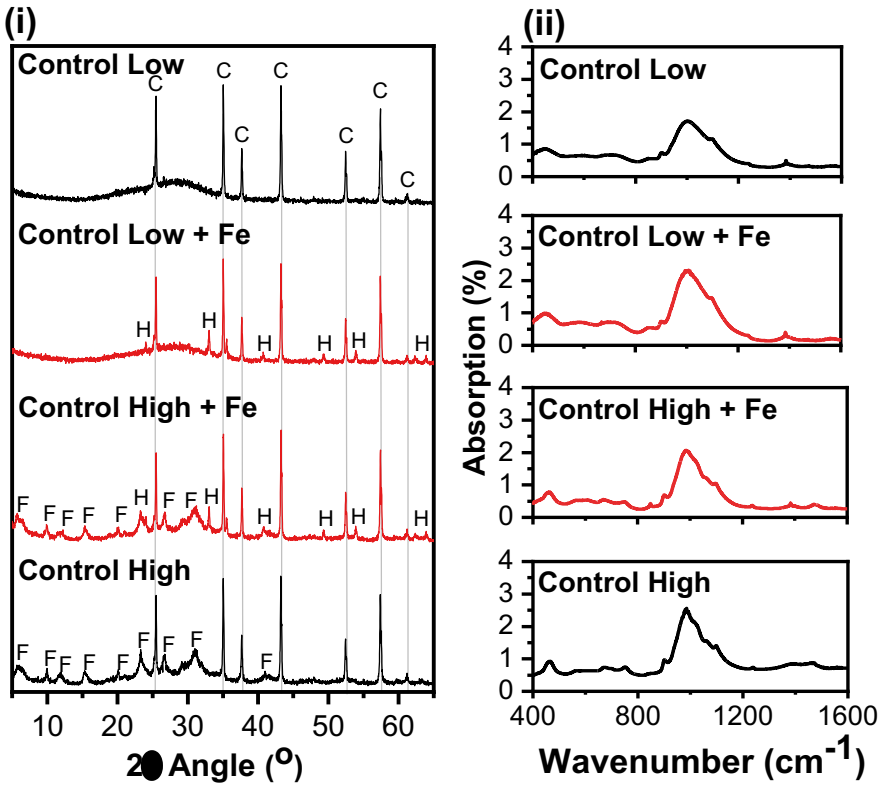

Figure 1. Mineralogy (i) and Fourier-transform infrared (FTIR) spectroscopy (ii) of all samples. In panel (i), F = faujasite ($Na_{2.06}Al_2Si_{3.8}O_{11.63}{\cdot}8H_2O$); H = hematite ($Fe_2O_3$); and, C = Corundum ($Al_2O_3$). Main Si-O-T band assignments for Control Low, Control Low + Fe, Control High, and Control High + Fe were 1005 cm^{-1}, 1006 cm^{-1}, 985 cm^{-1}, and 982 cm^{-1}, respectively.

No evidence was observed herein to indicate presence of a Fe-modified N-A-S-H cementitious binder (*i.e.*, Fe-O-Si bonds). Previous research has produced high-Fe alkali-activated materials from Fe-rich aluminosilicate precursors, such as laterite clays, Bayer red mud waste, and fayalitic slags. Contentious evidence has suggested, however, that high Fe content can result in (1) Si-O-Fe incorporation into the geopolymer network or (2) segregated formation of Fe octahedral phases [38]–[41]. Research has suggested that the consumption of Fe mineral phases leads to isomorphic substitution of Al by Fe ions, which possibly occurs in extremely distorted sites of gel-like phases. However, these results vary depending on precursor chemistry and dissolution kinetics associated with activating conditions [42]–[44]. Further research in similar metakaolin-based AACs as those studied here found no significant structural changes induced by hematite in similar metakaolin-based AACs [43], [45]. As a result, the FTIR data presented in **Figure 1(ii)** reveals no further structural evidence of Fe-O-Si bond formation.

3.2 Mineralogical and Structural Effects of Sulfuric Acid Exposure

After acid exposure, the mineral composition of all geopolymer samples remains largely identical to unexposed samples. Increases in faujasite formation were observed in samples with high alkali contents (**Figure 2(i)**). As expected, a loss of carbonates, Si, and Al was evidenced by FTIR band intensities (**Figure 2(ii)**). Carbonates are expected phases in N-A-S-H binders, due to the carbonation of alkalis (*e.g.*, Na^+) that remain after NaOH activation. In all geopolymer samples, carbonates exhibit some dissolution due to the low pH induced by sulfuric acid. This dissolution is evidenced in **Figure 2(ii)**, as a peak intensity decrease or absence in the 1384 cm^{-1} and 1560 cm^{-1} regions which correspond to O-C-O asymmetric stretching in carbonates [46], [47]. Notably absence of these peaks was observed in Control High samples, while Control

High + Fe samples retained the carbonate peak at 1384 cm^{-1}. This results indicate that these samples can conserve carbonates after sulfuric acid exposure. Further comparison between these spectra is presented in supplementary information, **Figure S.1**. This is important as the consumption of carbonates is expected to aid in arresting the protic dissolution of the Si-O-Al binder by serving as a pH buffering agent. For all Control Low formulations, regardless of Fe supplementation, structural modifications to the N-A-S-H binder, from a loss of Al (dealumination) and Na, is represented by a shift to higher wavenumbers, mainly from 999 cm^{-1} to ~1010 cm^{-1}, in the main Si-O-T band (1002 cm^{-1}) [48]–[51]. The relative peak intensity decrease renders other Si-O-Al symmetric stretching vibrations (670 cm^{-1}, 600 cm^{-1}, and, to a lesser extent, 590 cm^{-1}) peaks negligible indicating the loss of these Si-O-Al bonds most likely due to the dealumination of the material (**Figure S.1**). Control High samples with hematite addition remain largely unchanged after acid exposure, as evidenced by an increase in the main Si-O-T band (1002 cm^{-1}) intensity. However, a loss of a sharp peak at 850 cm^{-1} was observed after acid exposure indicating the deprotonation of silanols (Si-OH) bonds after acid attack [52]–[54]. The loss of silanols bonds may reflect a binder reorganization after acidic exposure, which could correlate with formation of faujasite as also shown in the XRD data due to an increase in the relative diffraction peak intensity (**Figure 2(i)**).

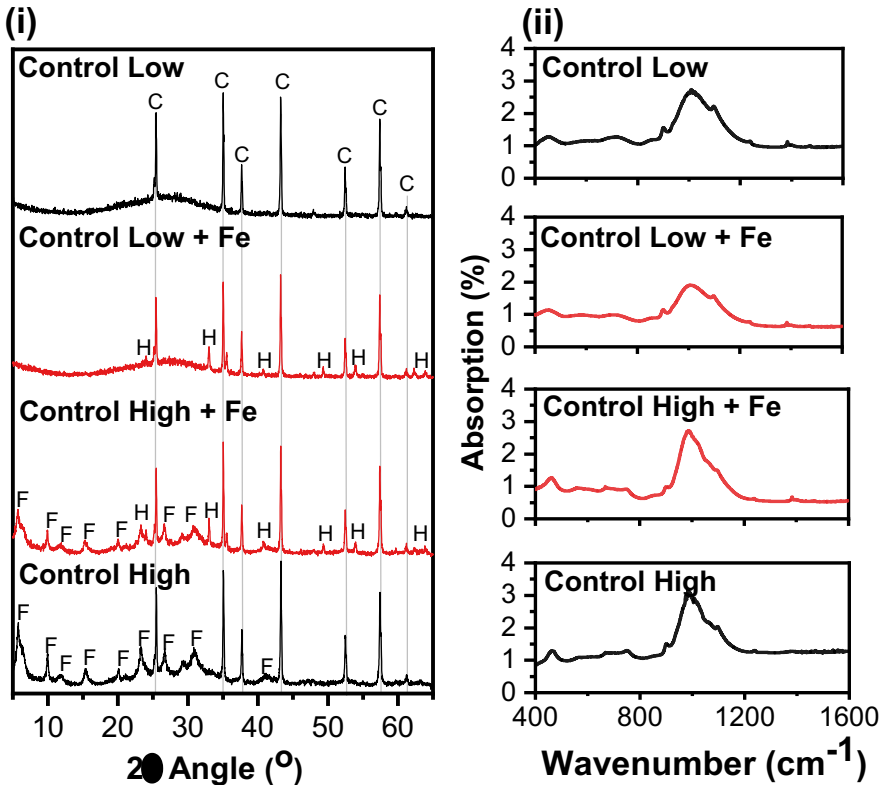

Figure 2. Acid exposed mineralogy (i) and Fourier-transform infrared (FTIR) spectroscopy (ii) of all samples. In panel (i) the "F" indicates the presence of faujasite ($Na_{2.06}Al_2Si_{3.8}O_{11.63}{\cdot}8H_2O$); "H" indicates the presence of hematite (Fe_2O_3); and, "C" indicates the presence of corundum (Al_2O_3).

Ion leaching profiles collected after three repeated sulfuric acid exposures are shown in **Figure 3**. Control Low samples without and with hematite addition bear no significant differences in Si, Na, and Fe leaching. However, slightly lower dealumination in the Control Low samples without hematite addition was observed. This result was supported by evidence obtained *via* FTIR (**Figure 2(ii)**). Contrastingly, Control High samples supplemented with hematite demonstrate up to 50% and 33% reductions in Si and Al leaching during acid exposure, respectively, confirming that hematite addition improves the acid resistance of these samples. The retention of these framework metals further substantiates the preservation

of the Si-O-Al bonds in the N-A-S-H cementitious binder and possible formation of Si-O-(Si) gels—a result also substantiated by FTIR data [49]. Na leaching in these samples is observed to be slightly higher at the third acid exposure. This result may indicate that Fe species could displace Na from local negative moieties (Al) in the N-A-S-H binder due to a higher chemical affinity. However, more research is necessitated to confirm this hypothesis.

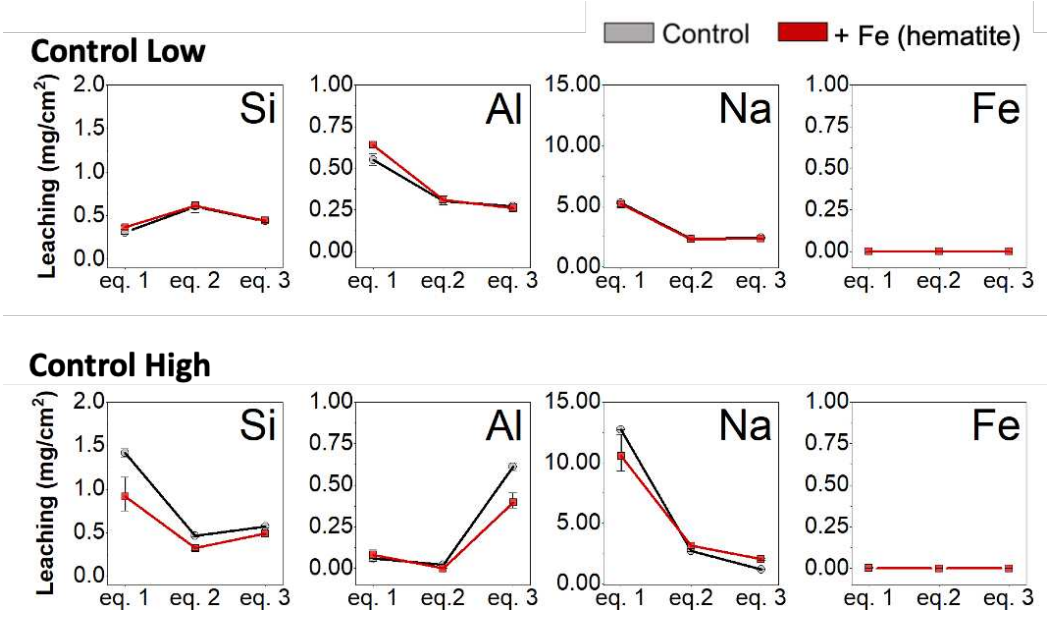

Figure 3. Normalized elemental leaching upon acid exposure for all sample formulations. Maximum and minimum leaching values are presented as lines, while average values are presented as squares.

The acid neutralization capacity of geopolymer samples after the first and second acid exposure is temporarily improved by an increase in hematite and alkali content (see **Table 2**). The acid neutralization capacity of samples is an important material property, as it demonstrates the ability of a material to buffer the pH of an acidic medium. The first acid exposure reveals that alkali content solely increases the acid neutralization capacity with higher final pH values for Control High formulations (12.43, 12.36) when compared to Control Low formulations (10.23, 10.59). As expected from earlier work on acid degradation of cementitious materials [48], [55]–[58]. After the second exposure, the addition of hematite increased the final pH from 4.10, as achieved by the Control High samples, to 5.27. This increase is likely due to the dissolution of hematite since lower Si leaching and minimal differences in dealumination are observed. However, by the third exposure, the acid neutralization capacity imparted by hematite is negligible. Minimal changes to the final pH were observed between samples without and with hematite (*i.e.*, 3.81 vs. 3.99). These data show that the acid resistance benefits of the Control High samples supplemented with Fe described by the mineralogy, molecular structure, and leaching data cannot be solely due to the acid buffering capacity of hematite-containing samples.

Table 2. Final pH value at each equilibrium exposure for all sample formulations.

Sample Name	Acid Exposure Cycle	Final pH
Control Low	1	10.23
	2	3.96
	3	3.96

Control Low + Fe	1	10.59
	2	3.95
	3	4.09
Control High	1	12.43
	2	4.10
	3	3.81
Control High + Fe	1	12.36
	2	5.27
	3	3.99

3.3 Physico-Mechanical Changes after Sulfuric Acid Exposure

Table 3 summarizes the observable (> 6 μm) segmented porosity of geopolymer samples before and after sulfuric acid exposure. The porosity of Control Low samples without and with Fe approximately doubled upon exposure to acid, thus confirming previous FTIR, XRD, and leaching results that, at low alkali contents, hematite addition reveals a negligible benefit to acid resistance. Increasing alkali content of geopolymer formulations, regardless of hematite addition, yields an increase in the original observable porosity. Upon sulfuric acid exposure, however, Control High samples with hematite additions do not reveal a significant change in porosity (1.11%). Hence, the changes to the molecular structure (*i.e.*, Si-rich gel formation and Si-O-Al preservation) minimally affect the porosity of Control High with hematite samples. Control High samples without hematite, however, structurally cracked excessively (structural failure) after acid exposure, probably due to the small sample size required for μ-CT analysis. The sample geometry may have increased the rate of deleterious sample desiccation and produce destructive diffusion-driven hydro-mechanical forces [59], [60].

Table 3. Cumulative visible porosity (> 6 μm) as determined by μ-CT scans of unexposed and acid exposed geopolymer samples. * Sample structurally failed with excessive cracking due to acid exposure.

Sample Name	Unexposed	S.D.	Exposed	S.D.
Control Low	0.73%	0.01%	1.30%	0.13%
Control Low + Fe	0.62%	0.01%	1.29%	0.09%
Control High	1.09%	0.02%	NA*	NA*
Control High + Fe	1.11%	0.03%	1.11%	0.03%

The compressive strength of all geopolymer samples before and after acid exposure is shown in **Figure 4**. For low Na:Al ratio samples, similar compressive strengths are observed prior to and upon acid exposure. Thus, no significant effect on the acid resistance was found for hematite supplements at low Na:Al formulations. This result corroborates previous experimental results obtained for low Na:Al samples. Aside from the slightly higher dealumination of Control Low with hematite samples, the Control Low samples with and without hematite do not differ significantly in molecular structure, mineralogy, observable porosity or, as evidenced in **Figure 4**, compressive strength.

Increasing the Na:Al content yields increased compressive strengths for geopolymer samples, as expected higher degrees of binder crosslinking **(Figure 1(ii)**). Hematite addition, however, reduced the unexposed compressive strength by ~29% in Control High samples. Recent research has demonstrated similar effects on mechanical performance, attributing iron phases with the formation of weak interfacial planes between the mineral and cementitious matrix [61]. Once acid-exposed, the compressive strength is

not significantly affected for Control High samples with hematite, indicating improved acid resistance. These results reveal the synergistic acid resistance benefits of higher alkali contents (Na:Al = 1.39) and hematite (5 wt.%). Contrastingly, compressive strength decreased by ~36% in the Control High samples without hematite upon exposure to acid.

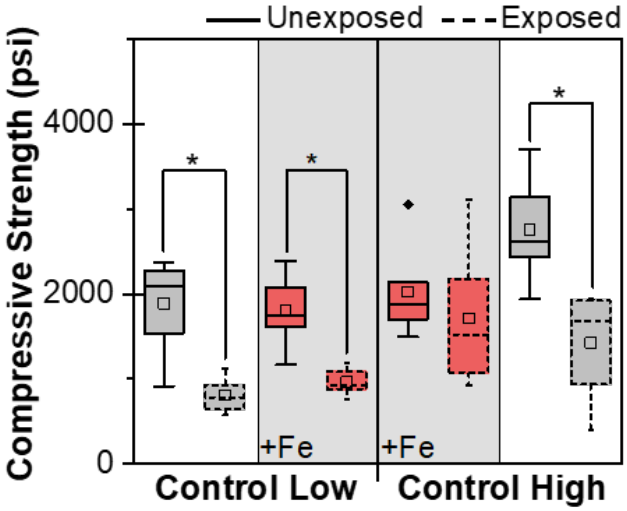

Figure 4. Compressive strength of all formulations. * Denotes statistically significant difference in the sample mean (p-value < 0.05).

3.4 Mechanisms of Acid Degradation in Geopolymers with Iron Mineral Admixtures

Results from EDS chemical mapping (see **Table 4**) suggest that hematite influences the acid degradation of the N-A-S-H cementitious binder and that this influence depends on the degree of Al crosslinking of the binder, which is affected by activating conditions (i.e., Na_2O wt.%). As observed in **Table 4**, acid exposure slightly changes the mean Si:Fe ratio of Fe-supplemented Control Low and Control High samples. However, these changes are minimal and reveal no statistical significance. The slight decrease in the mean Si:Fe ratio in Control High + Fe samples can be understood due to the high leaching of Si from these samples' formulations, see **Figure 3**. Expectedly, the Si:Al ratio increases in Control Low samples (**Table 4**) as a result of the dealumination of the material, observed in **Figure 3** and **Figure 2**. However, when hematite is present the Si:Al ratio of the microstructure is statistically similar after acid exposure. The unchanged Si and Al content in the acid-attacked microstructure was not indicative of the material's durability performance as this Fe-supplemented material revealed similar compressive strength as Control Low samples (**Figure 4**); indicating that hematite addition was likely not a contributor to the acid durability of these samples. Lastly, compressive strength benefits were observed for Control High + Fe samples (**Figure 4**) as well as both lower Si and Al leaching (**Figure 3**) and higher acid buffering capacities (**Table 2**). These acid resistance improvements are associated with a slight increase in the Fe:Al ratio within the microstructure (**Table 4**). In order to add more confidence to this correlated finding larger datasets must be analyzed.

Table 4. Microstructural stoichiometric ratios (Si:Al, Si:Fe, and Fe:Al) of geopolymer materials before (control) and after sulfuric acid exposure (acid). [A] statistically significant mean difference calculated with One-way ANOVA (p-value = 0.059). [B] p-value = 0.171, which is higher than the *a priori* p-value (0.05, 95% confidence).

	Si:Al		Si:Fe		Fe:Al	
Sample Name	**Control**	**Acid**	**Control**	**Acid**	**Control**	**Acid**

Control Low	1.27 [A]	1.30 [A]	-	-	-	-
Control Low + Fe	1.29	1.29	28.30	29.24	0.06	0.09
Control High	1.28	1.27	-	-	-	-
Control High + Fe	1.27	1.25	31.95	26.29	0.06 [B]	0.09 [B]

As discussed, the acid degradation behavior of samples was observed to vary depending on the degree of crosslinking in the cementitious binder and formation of secondary phases, such as faujasite zeolites. Chemical evidence gathered by EDS demonstrates increases of the central tendencies (*i.e.,* median, mean) for the Fe:Al ratio after sulfuric acid exposure (**Table 4)**. The formation of thermodynamically favorable Fe cationic molecules (*e.g.,* $FeSO_4^+$) may result in association with negatively charged moieties of the aluminosilicate network (Si-O-Al). As evidenced by leaching (**Figure 3**) and FTIR data (**Figure 2**), dealumination occurs in these samples, which creates a concomitant increase in negative moieties during protic electrophilic attack. During this process, the electrophilic attack may be arrested if released cationic species can stabilize the unstable negative moiety of the Si-O-Al network.

4. Conclusions

This study explains, for the first time, how iron mineral admixtures (*i.e.*, hematite) affect material properties prior to and after sulfuric acid exposure (pH = 2.00 ± 0.07) and how resultant microstructural effects can explain the acid resistance commonly observed in alkali-activated materials. Results indicate that iron phases, such as hematite, can improve the acid resistance in high Na:Al geopolymer formulations. Improved acid resistance resulted in lower compressive strength loss due to acid attack, lower increases in observable porosity, and an arrest of the degradation of the cementitious binder.

Hematite was observed to be inert during alkali activation. Prior to acid exposure, increasing the sodium content yielded expected formation of silicon-rich mineral phases (i.e., faujasite) as well as an increase in the extent of N-A-S-H binder network formation. No evidence for Fe-induced modification of the geopolymer cementitious binder was observed. Instead, weak bonding between the cementitious binder and hematite particles resulted in lower initial compressive strength.

After acid exposure, the addition of hematite was only observed to have a beneficial effect at high alkali contents (Na:Al = 1.39). Acid resistance was observed by (1) statistically insignificant loss of compressive strength, (2) minimal changes to the molecular structure (main Si-O-Al bond), (3) statistically insignificant changes to porosity, and (4) low leaching of Al (*i.e.*, dealumination) and Si. However, these results were not found true for samples with lower alkali contents (Na:Al = 0.86), most likely due to a lesser extent of Al-crosslinked N-A-S-H and lack of secondary mineral phases forming (i.e., zeolites).

The evidence collected and reported herein indicates that the acid buffering capacity of geopolymers, specifically at higher alkali content formulations, increases due to the addition of hematite. In turn, an increased buffering capacity leads to lower degrees of dealumination of the N-A-S-H cementitious binder.

5. Acknowledgments

This research was made possible by the Department of Civil, Environmental, and Architectural Engineering, the College of Engineering and Applied Sciences, and the Living Materials Laboratory at the University of Colorado Boulder. This work was supported by the United States National Science Foundation (Award No. CBET-1604457). Dr. Kate Campbell of the United States Geological Survey (USGS) is gratefully acknowledged for her insightful comments and discussions. Dr. J.P. Gevaudan's participation to complete this study was supported by the European Union's Horizon 2020 research and

innovation programme under the Marie Skłodowska-Curie grant agreement No. 839436. This study represents the views of the authors and not necessarily those of the sponsors. Any use of trade, firm, or product names was for descriptive purposes only and does not imply endorsement by the U.S. government.

6. Works Cited

[1] U.S. Environmental Protection Agency (EPA), "Clean Watersheds Needs Survey - Report to Congress," 2008.

[2] American Society of Civil Engineers (ASCE) Foundation, "2017 Wastewater Infrastructure Report Card," 2017.

[3] M. House and W. Weiss, "Review of microbially induced corrosion and comments on needs related to testing procedures," 2014.

[4] M. Abdulkareem, J. Havukainen, and M. Horttanainen, "How environmentally sustainable are fibre reinforced alkali-activated concretes?," *J. Clean. Prod.*, vol. 236, p. 117601, Nov. 2019, doi: 10.1016/j.jclepro.2019.07.076.

[5] N. Youssef, A. Z. Rabenantoandro, Z. Dakhli, F. H. Chehade, and Z. Lafhaj, "Environmental evaluation of geopolymer bricks," *MATEC Web Conf.*, vol. 281, p. 03005, 2019, doi: 10.1051/matecconf/201928103005.

[6] A. Dal Pozzo, L. Carabba, M. C. Bignozzi, and A. Tugnoli, "Life cycle assessment of a geopolymer mixture for fireproofing applications," *Int. J. Life Cycle Assess.*, vol. 24, no. 10, pp. 1743–1757, Oct. 2019, doi: 10.1007/s11367-019-01603-z.

[7] T. Bakharev, J. G. Sanjayan, and Y. B. Cheng, "Resistance of alkali-activated slag concrete to acid attack," *Cem. Concr. Res.*, vol. 33, no. 10, pp. 1607–1611, 2003, doi: 10.1016/S0008-8846(03)00125-X.

[8] M. Vafaei, A. Allahverdi, P. Dong, and N. Bassim, "Durability performance of geopolymer cement based on fly ash and calcium aluminate cement in mild concentration acid solutions," *J. Sustain. Cem.-Based Mater.*, vol. 8, no. 5, pp. 290–308, Sep. 2019, doi: 10.1080/21650373.2019.1615568.

[9] F. Pacheco-Torgal, J. Castro-Gomes, and S. Jalali, "Alkali-activated binders: A review: Part 1. Historical background, terminology, reaction mechanisms and hydration products," *Constr. Build. Mater.*, vol. 22, no. 7, pp. 1305–1314, Jul. 2008, doi: 10.1016/j.conbuildmat.2007.10.015.

[10] T. Bakharev, "Resistance of geopolymer materials to acid attack," *Cem. Concr. Res.*, vol. 35, no. 4, pp. 658–670, 2005, doi: 10.1016/j.cemconres.2004.06.005.

[11] H. Ye and L. Huang, "Degradation mechanisms of alkali-activated binders in sulfuric acid: The role of calcium and aluminum availability," *Constr. Build. Mater.*, vol. 246, p. 118477, Jun. 2020, doi: 10.1016/j.conbuildmat.2020.118477.

[12] H. A. Khan, M. S. H. Khan, A. Castel, and J. Sunarho, "Deterioration of alkali-activated mortars exposed to natural aggressive sewer environment," *Constr. Build. Mater.*, vol. 186, pp. 577–597, Oct. 2018, doi: 10.1016/j.conbuildmat.2018.07.137.

[13] B. Drugă, N. Ukrainczyk, K. Weise, E. Koenders, and S. Lackner, "Interaction between wastewater microorganisms and geopolymer or cementitious materials: Biofilm characterization and deterioration characteristics of mortars," *Int. Biodeterior. Biodegrad.*, vol. 134, pp. 58–67, Oct. 2018, doi: 10.1016/j.ibiod.2018.08.005.

[14] H. A. Khan, A. Castel, and M. S. H. Khan, "Corrosion investigation of fly ash based geopolymer mortar in natural sewer environment and sulphuric acid solution," *Corros. Sci.*, vol. 168, p. 108586, May 2020, doi: 10.1016/j.corsci.2020.108586.

[15] M. Vafaei, A. Allahverdi, P. Dong, and N. Bassim, "Acid attack on geopolymer cement mortar based on waste-glass powder and calcium aluminate cement at mild concentration," *Constr. Build. Mater.*, vol. 193, pp. 363–372, Dec. 2018, doi: 10.1016/J.CONBUILDMAT.2018.10.203.

[16] P. Duan, C. Yan, W. Zhou, W. Luo, and C. Shen, "An investigation of the microstructure and durability of a fluidized bed fly ash–metakaolin geopolymer after heat and acid exposure," *Mater. Des.*, vol. 74, pp. 125–137, 2015.

[17] P. Sturm, G. J. G. Gluth, C. Jäger, H. J. H. Brouwers, and H.-C. Kühne, "Sulfuric acid resistance of one-part alkali-activated mortars," *Cem. Concr. Res.*, vol. 109, pp. 54–63, Jul. 2018, doi: 10.1016/j.cemconres.2018.04.009.

[18] M. M. Komljenovic, Z. Bascarevic, N. Marjanovic, and V. Nikolic, "Decalcification resistance of alkali-activated slag," *J. Hazard. Mater.*, vol. 234, pp. 112–121, 2012, doi: 10.1016/j.jhazmat.2012.06.063.

[19] J. P. Gevaudan, A. Caicedo-Ramirez, M. T. Hernandez, and W. V. Srubar, "Copper and cobalt improve the acid resistance of alkali-activated cements," *Cem. Concr. Res.*, vol. 115, no. June, pp. 1–12, Jan. 2018, doi: 10.1016/j.cemconres.2018.08.002.

[20] S. You, S. W. Ho, T. Li, T. Maneerung, and C.-H. Wang, "Techno-economic analysis of geopolymer production from the coal fly ash with high iron oxide and calcium oxide contents," *J. Hazard. Mater.*, vol. 361, pp. 237–244, Jan. 2019, doi: 10.1016/J.JHAZMAT.2018.08.089.

[21] W. Shen, Y. Wang, T. Zhang, M. Zhou, J. Li, and X. Cui, "Magnesia modification of alkali-activated slag fly ash cement," *J. Wuhan Univ. Technol.-Mater Sci Ed*, vol. 26, no. 1, pp. 121–125, Feb. 2011, doi: 10.1007/s11595-011-0182-8.

[22] J. Osio-Norgaard, J. P. Gevaudan, and W. V. Srubar, "A review of chloride transport in alkali-activated cement paste, mortar, and concrete," *Constr. Build. Mater.*, vol. 186, pp. 191–206, Oct. 2018, doi: 10.1016/j.conbuildmat.2018.07.119.

[23] S. Mundra, D. P. Prentice, S. A. Bernal, and J. L. Provis, "Modelling chloride transport in alkali-activated slags," *Cem. Concr. Res.*, vol. 130, p. 106011, Apr. 2020, doi: 10.1016/j.cemconres.2020.106011.

[24] Y. K. Cho, S. H. Jung, and Y. C. Choi, "Effects of chemical composition of fly ash on compressive strength of fly ash cement mortar," *Constr. Build. Mater.*, vol. 204, pp. 255–264, Apr. 2019, doi: 10.1016/j.conbuildmat.2019.01.208.

[25] R. R. Lloyd, J. L. Provis, and J. S. J. van Deventer, "Acid resistance of inorganic polymer binders. 1. Corrosion rate," *Mater. Struct.*, vol. 45, pp. 1–15, 2012, doi: 10.1617/s11527-011-9744-7.

[26] C. Grengg, N. Ukrainczyk, G. Koraimann, B. Mueller, M. Dietzel, and F. Mittermayr, "Long-term in situ performance of geopolymer, calcium aluminate and Portland cement-based materials exposed to microbially induced acid corrosion," *Cem. Concr. Res.*, vol. 131, p. 106034, May 2020, doi: 10.1016/j.cemconres.2020.106034.

[27] A. Özcan and M. B. Karakoç, "The Resistance of Blast Furnace Slag- and Ferrochrome Slag-Based Geopolymer Concrete Against Acid Attack," *Int. J. Civ. Eng.*, vol. 17, no. 10, pp. 1571–1583, Oct. 2019, doi: 10.1007/s40999-019-00425-2.

[28] P. E. Tsakiridis, G. D. Papadimitriou, S. Tsivilis, and C. Koroneos, "Utilization of steel slag for Portland cement clinker production," *J. Hazard. Mater.*, vol. 152, no. 2, pp. 805–811, Apr. 2008, doi: 10.1016/j.jhazmat.2007.07.093.

[29] J. P. J. P. Gevaudan, K. M. K. M. Campbell, T. J. T. J. Kane, R. K. R. K. Shoemaker, and W. V. W. V. Srubar, "Mineralization dynamics of metakaolin-based alkali-activated cements," *Cem. Concr. Res.*, vol. 94, pp. 1–12, 2017, doi: 10.1016/j.cemconres.2017.01.001.

[30] F. Pacheco-Torgal, Z. Abdollahnejad, a. F. Camões, M. Jamshidi, and Y. Ding, "Durability of alkali-activated binders: A clear advantage over Portland cement or an unproven issue?," *Constr. Build. Mater.*, vol. 30, pp. 400–405, 2012, doi: 10.1016/j.conbuildmat.2011.12.017.

[31] A. Palomo, A. Fernández-Jiménez, and M. Criado, ""Geopolymers": same basic chemistry, different microstructures," *Mater. Construccion*, vol. 54, no. 275, pp. 77–91, 2004.

[32] P. Duxson, a. Fernández-Jiménez, J. L. Provis, G. C. Lukey, a. Palomo, and J. S. J. van Deventer, "Geopolymer technology: the current state of the art," *J. Mater. Sci.*, vol. 42, no. 9, pp. 2917–2933, 2007, doi: 10.1007/s10853-006-0637-z.

[33] J. Provis, "Geopolymers and other alkali activated material: why, how, what? ," *Materials and structures*, vol. 47, no. 11. p. 25, 2013.

[34] A. Hajimohammadi, J. L. Provis, and J. S. J. van Deventer, "The effect of silica availability on the mechanism of geopolymerisation," *Cem. Concr. Res.*, vol. 41, no. 3, pp. 210–216, Mar. 2011, doi: 10.1016/j.cemconres.2011.02.001.

[35] I. Ismail, S. A. Bernal, J. L. Provis, R. San Nicolas, S. Hamdan, and J. S. J. J. Van Deventer, "Modification of phase evolution in alkali-activated blast furnace slag by the incorporation of fly ash," *Cem. Concr. Compos.*, vol. 45, pp. 125–135, Jan. 2014, doi: 10.1016/j.cemconcomp.2013.09.006.

[36] S. A. Bernal, J. L. Provis, V. Rose, and R. Mej??a De Gutierrez, "Evolution of binder structure in sodium silicate-activated slag-metakaolin blends," *Cem. Concr. Compos.*, vol. 33, no. 1, pp. 46–54, 2011, doi: 10.1016/j.cemconcomp.2010.09.004.

[37] C. A. Rees, J. L. Provis, G. C. Lukey, and J. S. J. Van Deventer, "In situ ATR-FTIR study of the early stages of fly ash geopolymer gel formation," *Langmuir*, vol. 23, no. 17, pp. 9076–9082, 2007.

[38] D. S. Perera, J. D. Cashion, M. G. Blackford, Z. Zhang, and E. R. Vance, "Fe speciation in geopolymers with Si/Al molar ratio of ~2," *J. Eur. Ceram. Soc.*, vol. 27, no. 7, pp. 2697–2703, Jan. 2007, doi: 10.1016/J.JEURCERAMSOC.2006.10.006.

[39] R. C. Kaze *et al.*, "Microstructure and engineering properties of Fe2O3(FeO)-Al2O3-SiO2 based geopolymer composites," *J. Clean. Prod.*, vol. 199, pp. 849–859, Oct. 2018, doi: 10.1016/J.JCLEPRO.2018.07.171.

[40] C. R. Kaze *et al.*, "Effect of silicate modulus on the setting, mechanical strength and microstructure of iron-rich aluminosilicate (laterite) based-geopolymer cured at room temperature," *Ceram. Int.*, vol. 44, no. 17, pp. 21442–21450, Dec. 2018, doi: 10.1016/J.CERAMINT.2018.08.205.

[41] S. Onisei, A. P. Douvalis, A. Malfliet, A. Peys, and Y. Pontikes, "Inorganic polymers made of fayalite slag: On the microstructure and behavior of Fe," *J. Am. Ceram. Soc.*, vol. 101, no. 6, pp. 2245–2257, Jun. 2018, doi: 10.1111/jace.15420.

[42] P. N. Lemougna, K. J. D. MacKenzie, G. N. L. Jameson, H. Rahier, and U. F. Chinje Melo, "The role of iron in the formation of inorganic polymers (geopolymers) from volcanic ash: A 57Fe Mossbauer spectroscopy study," *J. Mater. Sci.*, vol. 48, no. 15, pp. 5280–5286, 2013, doi: 10.1007/s10853-013-7319-4.

[43] K. C. Gomes, G. S. T. Lima, S. M. Torres, S. R. de Barros, I. F. Vasconcelos, and N. P. Barbosa, "Iron distribution in geopolymer with ferromagnetic rich precursor," in *Materials Science Forum*, 2010, vol. 643, pp. 131–138.

[44] Y. Hu *et al.*, "Role of Fe species in geopolymer synthesized from alkali-thermal pretreated Fe-rich Bayer red mud," *Constr. Build. Mater.*, vol. 200, pp. 398–407, 2019.

[45] N. Essaidi, B. Samet, S. Baklouti, and S. Rossignol, "The role of hematite in aluminosilicate gels based on metakaolin," *Ceram. Silik.*, vol. 58, no. 1, pp. 1–11, 2013.

[46] C. Chen, C. Ho, and C. D. Chen, "Physicochemical Properties of Calcium Silicate Cements for Endodontic Treatment," *J. Endod.*, vol. 35, no. 9, pp. 1288–1291, 2009, doi: 10.1016/j.joen.2009.05.036.

[47] A. R. Davis and B. G. Oliver, "A vibrational-spectroscopic study of the species present in the CO2-H2O system," *J. Solut. Chem.*, vol. 1, no. 4, pp. 329–339, 1972, doi: 10.1007/bf00715991.

[48] A. Allahverdi and F. Škvára, "Nitric acid attack on hardened paste of geopolymeric cements. Part 2," *Ceram. - Silik.*, vol. 45, no. 4, pp. 143–149, 2001, doi: 10.1016/S0167-577X(02)01009-1.

[49] S. A. Bernal, E. D. Rodríguez, R. Mejía, R. Mejía De Gutiérrez, and J. L. Provis, "Performance of alkali-activated slag mortars exposed to acids Performance of alkali-activated slag mortars exposed to acids," *J. Sustain. Cem.-Based Mater.*, vol. 1, no. 3, 2012.

[50] W. G. Valencia-Saavedra, R. Mejía de Gutiérrez, and F. Puertas, "Performance of FA-based geopolymer concretes exposed to acetic and sulfuric acids," *Constr. Build. Mater.*, vol. 257, p. 119503, Oct. 2020, doi: 10.1016/j.conbuildmat.2020.119503.

[51] M. Zerzouri Lakhssassi, S. Alehyen, M. El Alouani, and M. Taibi, "The effect of aggressive environments on the properties of a low calcium fly ash based geopolymer and the ordinary Portland

cement pastes," *Mater. Today Proc.*, vol. 13, pp. 1169–1177, Jan. 2019, doi: 10.1016/j.matpr.2019.04.085.
[52] T. Uchino, T. Sakka, and K. Hotta, "Attenuated Total Reflectance Fourier-Transform Infrared," vol. 75, pp. 6–8, 1989.
[53] M. Zhang, Q. Hui, X. J. Lou, S. A. T. Redfern, E. K. H. Salje, and S. C. Tarantino, "Dehydroxylation, proton migration, and structural changes in heated talc: An infrared spectroscopic study," *Am. Mineral.*, vol. 91, no. 5–6, pp. 816–825, 2006, doi: 10.2138/am.2006.1945.
[54] B. Lafuente, R. T. Downs, H. Yang, and N. Stone, "The power of databases: The RRUFF project," in *Highlights in Mineralogical Crystallography*, T. Armbruster and R. M. Danisi, Eds. Berlin, Germany: De Gruyter, 2015, pp. 1–30.
[55] A. Allahverdi and F. Škvára, "Sulfuric acid attack on hardened paste of geopolymer cements-Part 1. Mechanism of corrosion at relatively high concentrations," *Ceram. - Silik.*, vol. 49, no. 4, p. 225, 2005.
[56] A. Allahverdi and F. Škvára, "Sulfuric acid attack on hardened paste of geopolymer cements Part 2. Corrosion mechanism at mild and relatively low concentrations," *Ceram. - Silik.*, vol. 50, no. 1, pp. 1–4, 2006, doi: 10.1016/S0167-577X(02)01009-1.
[57] A. Allahverdi and F. Škvára, "Nitric acid attack on hardened paste of geopolymeric cements. Part 1.," *Ceram. - Silik.*, vol. 45, no. 4, pp. 143–149, 2001, doi: 10.1016/S0167-577X(02)01009-1.
[58] A. Allahverdi and F. Škvára, "Acid Corrosion of Geopolymeric Cements," in *Seventh CANMET/ACI International Conference on fly ash, silica fume, and natural pozzolans in concrete*, 2001, vol. 2, pp. 561–579.
[59] T. Mohammadnejad and A. R. Khoei, "Hydro-mechanical modeling of cohesive crack propagation in multiphase porous media using the extended finite element method," *Int. J. Numer. Anal. Methods Geomech.*, vol. 37, no. 10, pp. 1247–1279, Jul. 2013, doi: 10.1002/nag.2079.
[60] J. A. Hudson, E. Liu, and S. Crampin, "The mechanical properties of materials with interconnected cracks and pores," *Geophys. J. Int.*, vol. 124, no. 1, pp. 105–112, 1996.
[61] S. C. Choi and W. K. Lee, "Effect of Fe2O3 on the physical property of geopolymer paste," in *Advanced Materials Research*, 2012, vol. 586, pp. 126–129.